P2.67

RETRIEVAL OF MICROPHYSICAL PROPERTIES OF SNOW USING SPECTRAL DUAL POLARIZATION ANALYSIS

A.L.J. Spek[1] D.N. Moisseev[2] H.W.J. Russchenberg[1*] C.M.H. Unal[1]
V. Chandrasekar[2]
[1] Delft University of Technology, IRCTR, Delft, The Netherlands
[2] Colorado State University, Fort Collins, Colorado

1 INTRODUCTION

Snow crystals consist of many different types of ice particles. Typical radar measurements observe only bulk properties of all types of ice particles present in a radar volume. Due to their difference in cross-section, large particles will reflect more power of the transmitted radar signal than small particles. If small and large particles are present in the same radar volume with comparable volume concentrations, the radar measurements will be dominated by larger particles. Because of this, it is difficult to obtain microphysical properties of both large and small particle types, based on reflectivity alone.

In this work, application of spectral dual polarization analysis for retrieval of microphysical properties of ice particles in stratiform precipitation is presented. Based on literature research a selection on the particle types that are predominantly present in radar measurements is done. The selection is based on radar cross-sections of the different particles and on meteorological conditions as well. The radar cross-sections are calculated with a model derived from literature. With the obtained knowledge, it is shown that only aggregates and plates dominate spectral radar retrievals above the melting layer of stratiform precipitation.

A model is created to simulate spectral radar observables of plates and aggregates. This model is dependent on the parameters of the drop size distribution of plates and aggregates, ambient wind velocity and spectral broadening. The simulated radar spectra are fitted to radar measurements using a non-linear least squares optimization technique. The data is obtained at the measurement site Cabauw, The Netherlands by TARA (Transportable Atmospheric Radar) (Heijnen et al. 2000). TARA is an S-band FM-CW dual polarization Doppler radar. The measurements are taken in stratiform precipitation. It is shown that under certain assumptions, the parameters of the drop size distributions of plates and aggregates, the ambient wind velocity and the spectral broadening can be retrieved from spectral radar measurements.

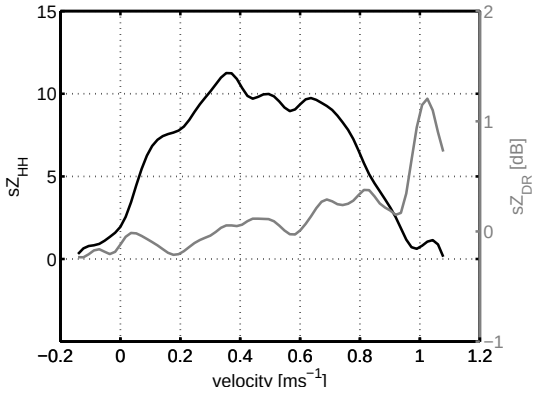

Figure 1: The goal of the work is to retrieve drop size distribution parameters of ice crystals in stratiform precipitation from spectral radar measurements

2 PROPERTIES OF SNOW PARTICLES

Previous research on ice particles came up with more than 60 different types of ice particles (Magono and Lee 1966). In this part of the work, properties of ice particles are given, which are necessary to determine the radar cross-sections of the different types. Important properties of the particles are size, shape, density, permittivity and fall velocity. Based on the derived radar

*Corresponding author address: H.W.J. Russchenberg, Delft University of Technology, IRCTR, Delft, The Netherlands. E-mail: H.W.J.Russchenberg@irctr.tudelft.nl

cross-sections, the particle types that dominate radar measurements are selected.

The different ice particle types given by Magono and Lee (1966), can be divided in three different groups, depending on their size. The most important ice particle types that represent the different groups are: plates, dendrites and columns for small ice particles; rimed particles and aggregates for the intermediate particles and graupel and hail for the large particles. An overview of these particles is given in figure 2.

The occurrence of the different ice particles depends on temperature, pressure and humidity of the atmosphere. Based on the atmospheric conditions above the melting layer during the measurements, it is not likely that columns are present (Gold and Power 1954). Next to that, the data is selected in a region well above the melting layer. With the assumption that no large updrafts are present, riming of ice particles is not likely.

Aggregates are a combination of pristine ice particles. Based on the shape of the particles, dendrites and plates have the largest chance to combine to another particle, which means that aggregates consist of a combination of plates and dendrites. This coincides also with the types of aggregates assumed in other research, see for example (Rajopadhyaya et al. 1994) and (Szymer and Zawadzki 1999).

A summary of the ice particle types that may be present, can be found in table 1. The sizes of the different particles, that are presented in the table as well, are typical sizes found in literature ((Mitchell et al. 1990), (Mitchell 1996) and (Pruppacher and Klett 1978)). It has to be taken into account that these boundaries aren't strict boundaries, which means that it is also possible that particles exist outside these boundaries.

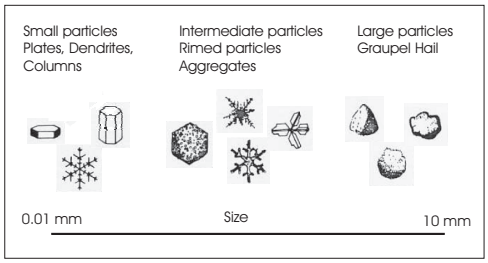

Figure 2: Typical forms of snow in the different size regions (Magono and Lee 1966)

Table 1: Types and typical sizes of snow particles

Type	Diameter [mm]
Plates	$0.015 \lesssim \mathrm{D} \lesssim 3$
Dendrites	$0.3 \lesssim \mathrm{D} \lesssim 4$
Aggregates	$0.5 \lesssim \mathrm{D} \lesssim 8$
Graupel	$2 \lesssim \mathrm{D} \lesssim 8$
Hail	$5 \lesssim \mathrm{D} \lesssim 25$

2.1 *Shape of the ice crystals*

It is very common to model the shape of hydrometeors as oblate spheroids, with the exception of graupel, which has a conical shape (Wang 1982).

Spheroidal shape According to Matrosov et al. (1996), the shape of snow crystals can be approximated by an oblate spheroid. The relation between the smallest and biggest particle dimensions are given by a power law,

$$w(D) = \xi D^{\zeta} \tag{1}$$

where w is the smallest dimension of the spheroid, and D the largest dimension. Values for ξ and ζ can be found in (Matrosov et al. 1996) and (Auer and Veal 1970) for plates, dendrites and aggregates. The relation for hail is given by Bringi and Chandrasekar (2001). All parameters used in this work are summarized in the appendix.

Conical shape A conical shape can be described by (Wang 1982),

$$x, y = \pm a[1 - (z^2/C^2)]^{\frac{1}{2}} \cos^{-1}(z/\lambda C) \tag{2}$$

where x, y and z are the coordinates of the surface and λ is a shape parameter and assumed to be equal to 2, according to Wang (1982). C is equal to half the intersection of the particle with the z axis and it can easily be verified that L equals π/a and $2x$ (Wang 1982). The relation between C and L is assumed to be constant for all diameters and is equal to $L = 0.9C$, according to Wang (1982).

Based on equations (1) and (2) the axis ratio, defined as the ratio of smallest and largest particle dimension, can be determined. In figure 3, the axis ratio is given as function of particle size. As can be seen in the figure,

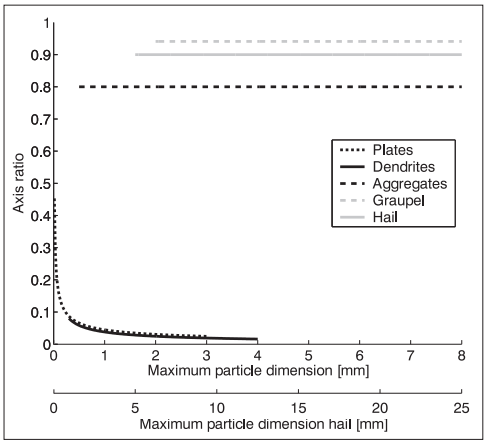

Figure 3: Dependence of axis ratio on particle size for different ice particles.

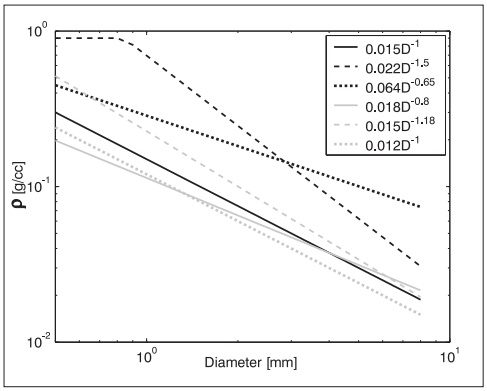

Figure 4: Different density relations for aggregates, dependent on diameter.The different relations are investigated in (Fabry and Szymer 1999). In this work, it is concluded the relation ρ=0.015D^{-1} fits reality best.

the axis ratio of hail, graupel and aggregates is constant over diameter. In reality these particles have very irregular shapes. It is common to fit these irregular shapes into spheroids, which are close to spheres, to simplify calculations. From the figure, it can also be noticed that plates and dendrites have a more oblate shape.

2.2 *Density of the ice crystals*

The density of ice particles can be modeled, according to Pruppacher and Klett (1978), as function of maximum particle dimension D,

$$\rho_e = kD^l \tag{3}$$

Pruppacher and Klett (1978) gives values for the variables k and l for plates and dendrites. The density for conical graupel and hail is taken from El-Magd et al. (2000). Because aggregates occur in many different appearances, their density is very difficult to model. However, Fabry and Szymer (1999) provide a comparison on the density relations found in literature and gives a relation which reproduces reality best. The relations investigated in (Fabry and Szymer 1999) are given in figure 4. The diameter-density relations for the different particles are given in figure 5.

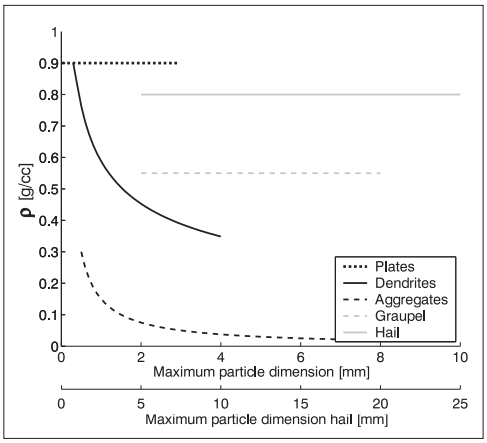

Figure 5: Dependence of particle density on particle size for different ice particle types.

2.3 *Relative permittivity of the ice crystals*

The different ice particle types all consist of a different mixture of air and ice, which has an effect on their density as can be seen in figure 5. The permittivity for these mixtures of air and ice can be calculated using

the Maxwell-Garnett formula (Bringi and Chandrasekar 2001). This equation gives the effective dielectric constant for mixtures depending on their volume concentrations. This formula calculates the dielectric constant based on the volume concentration of ice in air.

$$\begin{aligned} \frac{\epsilon_{\text{eff}}}{\epsilon_{air}} &= \frac{1+2cF}{1-cF} \\ F &= \frac{\epsilon_{ice}-\epsilon_{air}}{\epsilon_{ice}+2\epsilon_{air}} \\ c &= \frac{\rho_{particle}}{\rho_{ice}}\epsilon_{ice} \end{aligned} \tag{4}$$

with ϵ_{eff} the permittivity of the ice particle, c the volume concentration of the inclusion of ice in air, ϵ_{ice} and ϵ_{air} are the permittivities of ice and air respectively.

The permittivity of ice is dependent on temperature and frequency. Ray (1972) gives a way to calculate the permittivity of ice over a broad spectral range. The imaginary part of the dielectric constant is very small (1%) compared to the real part and is therefore neglected.

Due to the high correlation of permittivity with density, the figure of the permittivity-size relation is comparable to figure 5 and is therefore not provided.

2.4 *Velocity of the ice crystals*

The derivation of terminal fall velocity of hydrometeors is taken from (Mitchell 1996).

When an ice particle falls, an aerodynamic drag force acts upon it. This drag force is given by

$$F_D = \frac{1}{2}\rho_a v^2 A C_D \tag{5}$$

where v is the velocity, A the area projected to the normal flow of the ice particle. ρ_a is the density of air, and C_D is the drag coefficient.

The drag force acting upon the particle is equal to the gravitational force, which gives a terminal velocity of

$$v_t = \left(\frac{2mg}{\rho_a A C_D}\right)^{\frac{1}{2}} \tag{6}$$

where m is the mass of the particle and g is the gravitational constant. However, using this equation is difficult because it is not possible to characterize the drag coefficient independently of velocity (Mitchell 1996).

Therefore, in practice, the terminal velocity is often calculated by making use of Best (X) and Reynolds (Re) number. They are given by

$$X = \frac{2mg\rho_a D^2}{A\eta^2} \tag{7}$$

$$Re = \frac{vD\rho_a}{\eta} \tag{8}$$

where D is the largest dimension of the particle and η is the dynamic viscosity of air. Best number gives a relation for the microphysical properties of the ice particle and Reynolds number is related to velocity and the viscous forces on the ice particle. Relating Best and Reynolds number makes it possible to establish a relation between the microphysical properties and the velocity of the particle. Many experimental studies have shown, according to Mitchell (1996), that this relation exists and is given by a power law,

$$Re = aX^b \tag{9}$$

Combining equations [6-9], the terminal velocity is given by

$$v_t = \frac{a\nu}{D}\left(\frac{2mD^2 g}{\rho_a \nu^2 A}\right)^b \tag{10}$$

where is made use of the property $\nu = \eta/\rho_a$, which is the kinematic viscosity of air.

To obtain speed-size relations of ice particles dependent on their diameter, mass and area of these particles need to be parameterized as a function of diameter. For these parameterizations power laws are used (Mitchell 1996). They can be expressed as a function of maximum particle dimension D,

$$m(D) = \alpha D^\beta \tag{11}$$

$$A(D) = \gamma D^\sigma \tag{12}$$

Combining equations [10-12], the following equation is obtained for the terminal velocity of ice particles,

$$v_t = a\nu\left(\frac{2\alpha g}{\rho_a \nu^2 \gamma}\right)^b D^{b(\beta+2-\sigma)-1} \tag{13}$$

The values of α, β, γ and σ, for the different types of ice particles (except conical graupel), can be found in Mitchell (1996). The values for conical graupel are given by Heymsfield and Kajikawa (1987).

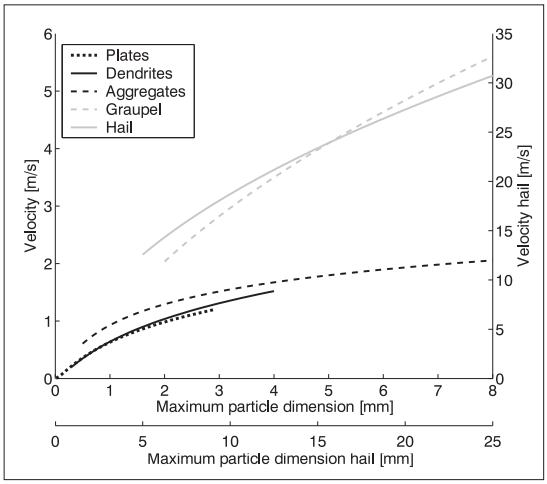

Figure 6: Velocity for different ice particles depending on their size.

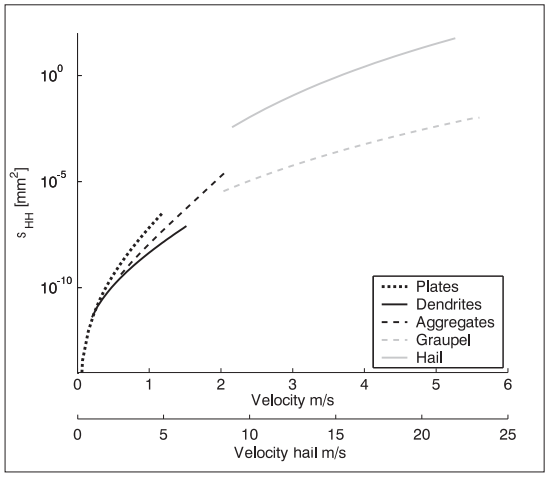

Figure 7: Radar cross-section for different ice particles types depending on their velocity. The elevation angle is 45^o and the frequency is 3 GHz

The values of a and b are derived in (Khvorostyanov and Curry 2002) as continuous function of X over the whole dimension range of the ice particles.

$$b(X) = \frac{\frac{1}{2}c_1 X^{\frac{1}{2}}}{\left[\left(1+c_1X^{\frac{1}{2}}\right)^{\frac{1}{2}}-1\right]\left(1+c_1X^{\frac{1}{2}}\right)^{\frac{1}{2}}} \quad (14)$$

$$a(X) = \frac{\sigma_0^2}{4}\left[\left(1+c_1X^{\frac{1}{2}}\right)^{\frac{1}{2}}-1\right]^2 X^{-b(X)} \quad (15)$$

where σ_0 and c_1 are constants.
Now a relation is derived for velocity dependent on maximum particle dimension D,

$$v_t(D) = AD^B \quad (16)$$

$$A = a\nu\left(\frac{2\alpha g}{\rho_a \nu^2 \gamma}\right)^b \quad (17)$$

$$B = b(\beta+2-\sigma)-1 \quad (18)$$

The fall velocities for the different particle types are shown in figure 6. From this plot it can be concluded that the different particles exist in different velocity regions. In the velocity region 0-2 ms^{-1} only plates, dendrites and aggregates exist. Graupel is observed in the region above 2 ms^{-1} and hail exists above 10 ms^{-1}.

2.5 *Selection of particle types*

With the given description of the properties of snow particles, it is possible to calculate the radar cross-section of the different types of snow particles, using Rayleigh scattering theory for spheroidal particles (Russchenberg 1992) and the T-matrix method for conical shaped particles (Mishchenko et al. 2000). The radar cross-section for the different types of snow particles depending on their velocity is given in figure 7.

Selection based on cross-sections Radar retrievals of precipitation are commonly expressed in the radar observables horizontal reflectivity and differential reflectivity. If only one type of particle is present in the radar volume, the spectral representations are given by (Skaropoulos and Russchenberg 2003),

$$sZ_{HH}(v)dv = N(D\{v\})\sigma_{HH}(D\{v\})\left|\frac{dD}{dv}\right|dv \quad (19)$$

$$sZ_{DR}(v)dv = \frac{N(D\{v\})\sigma_{HH}(D\{v\})\left|\frac{dD}{dv}\right|dv}{N(D\{v\})\sigma_{VV}(D\{v\})\left|\frac{dD}{dv}\right|dv} \quad (20)$$

Because the drop size distribution, N(D), and the radar cross-section are given as functions of diameter, the Jacobian $\left|\frac{dD}{dv}\right|$ is needed to take the change of variables, from diameter to velocity, into account.

As already stated, precipitation above the melting layer consists of multiple particle types and the radar observables are therefore given by a summation over

the n types present in the radar volume,

$$sZ_{HH}(v)dv = \sum_{i=1}^{n} N(D_i\{v\})\sigma_{HH,i}(D_i\{v\}) \left|\frac{dD}{dv}\right| dv \quad (21)$$

$$sZ_{DR}(v)dv = \frac{\sum_{i=1}^{n} N(D_i\{v\})\sigma_{HH,i}(D_i\{v\}) \left|\frac{dD}{dv}\right| dv}{\sum_{i=1}^{n} N(D_i\{v\})\sigma_{VV,i}(D_i\{v\}) \left|\frac{dD}{dv}\right| dv} \quad (22)$$

From equation (21) it can be concluded that if the number of particles of different particle types are the same and one of the respective radar cross-sections is significantly smaller, the scattering by this particle type will not be noticed.

Referring to figure 7, where the different cross-sections are shown, the following can be concluded:

- The radar cross-section of plates is significantly larger than the radar-cross section of dendrites for larger diameters.
- For small diameters their radar cross-sections become similar. Though, the microphysical properties for plates and dendrites are similar in this region as well (see figures 3, 5 and 6).

The second conclusion can be imagined easily as well, if dendrites become very small there will be hardly any air between the branches and the dendrite will look like plate crystals.

Because it is not likely that concentrations of dendrites and plates will be significantly different from each other (Cotton 2004), the radar backscattering from an ensemble of plates and dendrites will be dominated by plates and dendrites will not be noticed.

Selection based on velocity During the measurements with TARA only low fall velocities and spectral widths are observed. Considering the high fall velocity of hail and graupel, it is not likely that hail and graupel will be present in the radar data. Therefore they are excluded from the model from now on.

This leaves only plates and aggregates as particle types that dominate the radar retrievals. It has to be kept in mind that if higher velocities are observed the scattering by graupel and hail also effects the radar retrievals.

3 RETRIEVAL OF DSD PARAMETERS

In this part an algorithm is developed which extracts microphysical properties of plates and aggregates from spectral radar measurements above the melting layer in stratiform precipitation. The model described above, is extended to a model which produces the spectral moments. These simulated spectra are fitted to the measurements using a non-linear least squares optimization.

Using (21) and (22), spectral radar observables of precipitation above the melting layer can be created. To be able to create spectra, a suitable form of the drop size distribution has to be selected first. In literature, two forms of drop size distributions are commonly used, the gamma distribution and the exponential distribution. The main difference between these two distributions is an extra shape parameter which is included in the gamma distribution to take deviations into account for small particles. In the exponential distribution this shape parameter is set to zero.
Since both distributions are generally accepted and there is no well defined argument to prefer one above the other, the exponential distribution is used in this work. The main reason is, the parameters of the drop size distribution have to be retrieved by a retrieval algorithm. This will be significantly more easy if one degree of freedom is left out. However, there is no good reason to set the shape parameter to zero instead of e.g four. Therefore dependence on the choice of the shape parameter has to be investigated at a later stage.

The exponential distribution is given by

$$N(D) = N_w \exp\left[-(3.67)\frac{D}{D_0}\right] \quad (23)$$

with N_w the intercept parameter [mm^{-1}m^{-3}] and D_0 the median volume diameter [mm].

Because radar measurements are affected by spectral broadening, this parameter is included in the model as well. According to Doviak and Zrnic (1993), spectral broadening can be modeled as a convolution of the spectral radar observables with a gaussian convolution kernel,

$$sZ_{HHmod}(v) = sZ_{broad}(v) * sZ_{HH}(v) = \frac{1}{\sqrt{2\pi}\sigma_0}\int \exp\left[-\frac{(v-\tilde{v})^2}{2\sigma_0^2}\right] sZ_{HH}(v)d\tilde{v} \quad (24)$$

where $*$ denotes the convolution operator, σ_0 is the width of the broadening spectrum [ms^{-1}] and sZ_{HH} the spectrum given by equation (21).

A final parameter which effects radar measurements is ambient wind velocity. Due to wind velocity the observed velocity is shifted with respect to the real fall velocity by

$$v_{obs} = v_{fall} + v_0 \tag{25}$$

The description given above, gives a model for spectral radar observables dependent on 6 parameters,

$$sZ_{HH}^{mod} = sZ_{HH}(v, N_w^{agg}, D_0^{agg}, N_w^{pla}, D_0^{pla}, v_0, \sigma_0) \tag{26}$$

$$sZ_{DR}^{mod} = sZ_{DR}(v, N_w^{agg}, D_0^{agg}, N_w^{pla}, D_0^{pla}, v_0, \sigma_0) \tag{27}$$

3.1 *Dependence on DSD parameters*

To get insight in the dependence of sZ_{HH} and sZ_{DR} on the 6 parameters given in (26) and (27) a sensitivity study is carried out. By changing the parameters one by one, and keeping the other five constant, a good insight can be provided on the dependence of the radar observables on the different parameters.

In figures 8-10 the plots are shown for changing the different variables over a realistic range. The plots on the dependence of v_0 are left out because v_0 only generates a shift of the spectrum which can be easily imagined. From the figures the following can be concluded:

- An increase in N_w for aggregates leads to an increase in sZ_{HH} and a decrease in sZ_{DR}. The more aggregates there are, the more the total sZ_{DR} tends to the differential reflectivity of aggregates, which is close to zero dB, due to the near spherical shape of aggregates (see figure 3).
- An increase in D_0 for aggregates leads to an increase and a wider spectrum for sZ_{HH}. sZ_{DR} decreases for the same reason as explained for a change in N_w because the contribution of aggregates to the total spectrum becomes more dominant.
- An increase in N_w for plates hardly effects the observed sZ_{HH}. This is due to the fact that the radar cross-section for plates is significantly smaller with respect to the cross-section of aggregates (see figure 7). On the other hand sZ_{DR} increases with an increasing N_w. This is a result of the high sZ_{DR} for plates due to their oblate shape

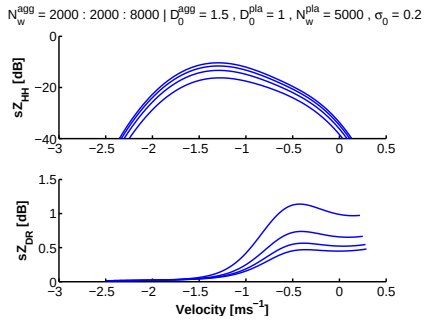

(a)

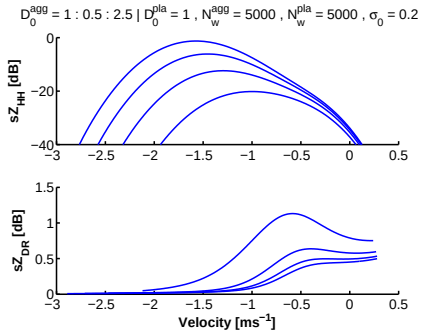

(b)

Figure 8: Dependence of sZ_{HH} and sZ_{DR} on the parameters of the drop size distribution for aggregates. Units are mm for D_0, mm^{-1}m^{-3} for N_w and ms^{-1} for σ_0.

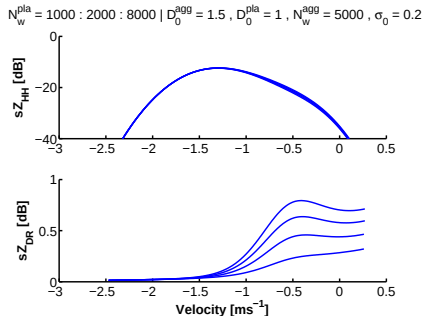

(a)

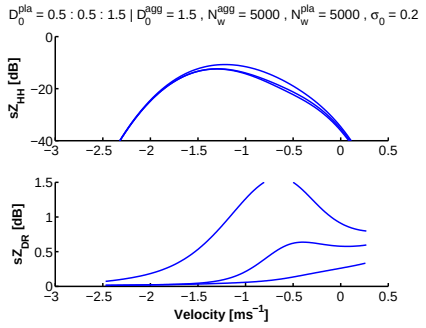

(b)

Figure 9: Dependence of sZ_{HH} and sZ_{DR} on the parameters of the drop size distribution for plates. Units are mm for D_0, $\text{mm}^{-1}\text{m}^{-3}$ for N_w and ms^{-1} for σ_0.

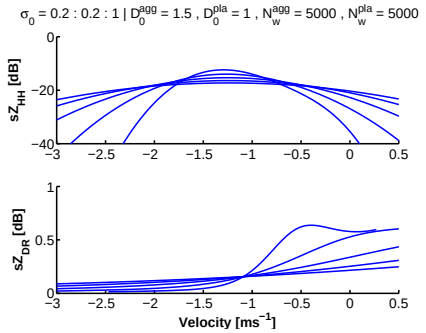

Figure 10: Dependence of sZ_{HH} and sZ_{DR} on the spectral broadening factor. Units are mm for D_0, $\text{mm}^{-1}\text{m}^{-3}$ for N_w and ms^{-1} for σ_0.

(see figure 3). With an increasing participation of plates in the observed differential reflectivity it tends more to the differential reflectivity of plates.

- An increase in D_0 for plates generates a similar effect as an increase of N_w for plates.
- The effect of spectral broadening on horizontal reflectivity is that the maximum of the spectrum becomes lower and the spectrum becomes wider and more symmetric as well. Next to that, an increase of spectral broadening flattens the profile of differential reflectivity.

3.2 *Retrieval of parameters*

With spectra created by (26) and (27), it is possible to develop a retrieval algorithm which obtains the six parameters from sZ_{HH} and sZ_{DR}. The parameters will be retrieved by fitting simulated spectra to measured spectra. Therefore an optimization can be used which minimizes the difference between the fitted spectrum and the measured spectrum by varying the six input parameters,

$$\min_{\substack{D_0^{agg},\ D_0^{pla},\ \sigma_0,\\ N_w^{agg},\ N_w^{pla},\ v_0}} \sum_{v=v_{min}}^{v_{max}} \left[sZ_{XX}^{meas}(v) - sZ_{XX}^{mod}\right]^2 \tag{28}$$

where the 'XX' denotes spectral horizontal reflectivity or spectral differential reflectivity. This minimization can be done using a non-linear least squares algorithm which minimizes the error,

$$\text{error}(\Psi) = \sum \left[sZ_{XX}^{meas}(v) - sZ_{XX}^{mod}(v,\Psi)\right]^2 \tag{29}$$

where Ψ is a vector containing all six parameters. The error as function of Ψ is often called the cost function.

Such six parameter non-linear least squares optimizations are very difficult to solve and time consuming. Therefore it is necessary to simplify (28). For that, the knowledge obtained on the dependence of the spectral radar observables on the six parameters will be used. From figures 8-10 it can be concluded, the shape of sZ_{HH} is largely determined by the drop size distribution parameters of aggregates, ambient wind velocity and spectral broadening. sZ_{DR} on the other hand, is determined by a combination of all six parameters. Therefore, a good approach to simplify (28) is to separate the six parameter optimization into two stages,

- determining the DSD parameters of aggregates,

ambient wind velocity and spectral broadening based on sZ_{HH}

- determining the DSD parameters of plates on sZ_{DR} using retrieved values from previous step

Optimization based on sZ_{HH} This separation simplifies the six parameter optimization into a four and a two parameter optimization. The first routine is given by

$$\min_{\Lambda} \sum \left[sZ_{HH}^{meas}(v) - sZ_{HH}^{mod}(v, \Lambda) \right]^2 \quad (30)$$

where Λ is a vector containing N_w^{agg},D_0^{agg},σ_0 and v_0. And the second optimization is given by

$$\min_{\Gamma} \sum \left[sZ_{DR}^{meas}(v) - sZ_{HH}^{mod}(v, \Gamma)|_{\Lambda} \right]^2 \quad (31)$$

with Γ a vector containing D_0^{pla} and N_w^{pla}.

The 4 parameter optimization can even by simplified to a two parameter optimization by separating N_w^{agg} and v_0 from D_0^{agg} and σ_0.

N_w^{agg} can be set apart from the other parameters by rewriting equation (30) to

$$sZ_{HH}^{meas} = sZ_{HH}^{mod}(v, 1, D_0^{agg}, v_0, \sigma_0) N_w^{agg} + \epsilon \quad (32)$$

where ϵ are random errors. The equation above, is just a linear combination of two vectors and therefore solvable using a least squares solution. (Equation 31 can be simplified in a similar way to a one parameter optimization over D_0^{pla}.)

Now assuming D_0^{agg}, N_w^{agg} and σ_0 to be known, v_0 can be estimated by calculating a reference spectrum with v_0 equal to zero and determining the lag of the cross-correlation between the measured spectrum and the reference spectrum

$$v_0 = \max \left\{ sZ_{HH}^{mod}(v, N_w^{agg}, D_0^{agg}, \sigma_0) \star sZ_{HH}^{meas}(v) \right\} \quad (33)$$

where $\star$ denotes the cross-correlation.

To be able to get insight in the quality of the described optimization routine, the error between a simulated spectrum and a fitted spectrum is calculated varying D_0^{agg}. This error is given by

$$\text{error}(\Lambda) = \sum \left[sZ_{HH}^{sim}(v) - sZ_{HH}^{mod}(v, \Lambda) \right]^2 \quad (34)$$

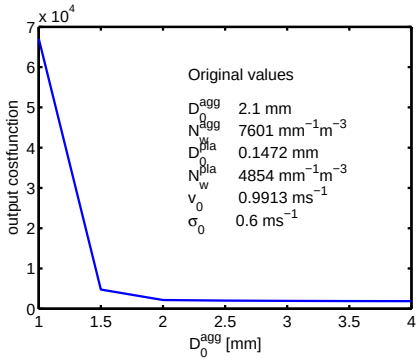

Figure 11: Example of output of cost function give by (34).

It turns out that this cost function has no unique minimum as is illustrated with figure 11. This is due to the fact that for increasing D_0^{agg} the spectral horizontal reflectivity becomes too symmetric. Therefore there is too little difference in spectra obtained for different D_0^{agg} and as a consequence, the error between simulated and fitted spectrum will be constant over D_0^{agg}.

Unfortunately, the output of the cost function of (30) has no minimum even if D_0^{pla} is known. This means that if a minimization is performed there is no guarantee the correct values of the six parameters will be obtained.

Optimization based on sZ_{DR} Because the described routine didn't give satisfactory results, a different approach to solve (28) is needed. Instead of defining a cost function based on sZ_{HH}, the error between measured and fitted spectral differential reflectivity will be minimized. This routine is given by

$$\min_{\Psi} \sum \left[sZ_{DR}^{meas}(v) - sZ_{DR}^{mod}(v, \Psi) \right]^2 \quad (35)$$

Again this routine will be splitted up for simplification. N_w^{agg}, N_w^{pla} will be calculated comparable to (32), though calculation is now based on sZ_{DR}

$$sZ_{DR}^{meas} = \frac{\sum_{n=1}^{2} sZ_{HH}^{mod}(v, 1, D_0^n, v_0, \sigma_0) N_w^n}{\sum_{n=1}^{2} sZ_{VV}^{mod}(v, 1, D_0^n, v_0, \sigma_0) N_w^n} + \epsilon \quad (36)$$

where the summation is done over the two particle types, aggregates and plates.

Comparable to equation 33, v_0 is calculated by

$$v_0 = \max \left\{ sZ_{HH}^{mod}(v, \Psi) \star sZ_{HH}^{meas}(v) \right\} \quad (37)$$

It turned out, the retrieval routine works best if optimization of σ_0 is separated from D_0^{agg} and D_0^{pla}. So, assuming all six parameters except σ_0 to be known, σ_0 can be calculated by the least squares optimization of

$$\min_{\sigma_0} \sum \left[sZ_{HH}^{meas}(v) - sZ_{HH}^{mod}(v, \Psi) \right]^2 \qquad (38)$$

The total routine is now given by

$$\min_{D_0^{agg}, D_0^{pla}} \min_{\sigma_0} \min_{v_0} \min_{N_w^{agg}, N_w^{pla}} \sum \left[sZ_{DR}^{meas}(v) - sZ_{DR}^{mod}(v, \Psi) \right]^2 \qquad (39)$$

with the optimization for σ_0 and v_0 based on sZ_{HH}.

3.3 *Quality of retrieval technique*

To test the quality of the retrieval technique the routine is applied to simulated spectra obtained with (26) and (27). To generate signals with real statistical properties, noise is added according to Chandrasekar et al. (1986). The values of the parameters are changed in the regions given in table 2.

Table 2: Regions of variables

Parameter	Region	
D_0^{agg}	0.5 - 3	mm
N_w^{agg}	0 - 8000	$\text{mm}^{-1}\text{m}^{-3}$
D_0^{pla}	0.2 - 1.8	mm
N_w^{pla}	0 - 8000	$\text{mm}^{-1}\text{m}^{-3}$
σ_0	0.1 - 0.7	ms^{-1}
v_0	0 - 1	ms^{-1}

It has to be noted that the estimation of the variables is only executed if sZ_{HH} exceeds -15 dB and if sZ_{DR} is larger than 0.6 dB. The first threshold is to ensure the spectrum has a sufficient signal-to-noise ratio to perform the optimization. The second threshold is to ensure that the amount of plates is detectable.

In figures 12-14 the results of the optimization for the six parameters are shown. On the horizontal axes the input parameter values are given and the retrieved values are plotted on the vertical axes.

4 APPLICATION TO TARA DATA

The developed retrieval technique is also applied to real measurements. These measurements are taken in a stratiform precipitation by TARA at Cabauw, The

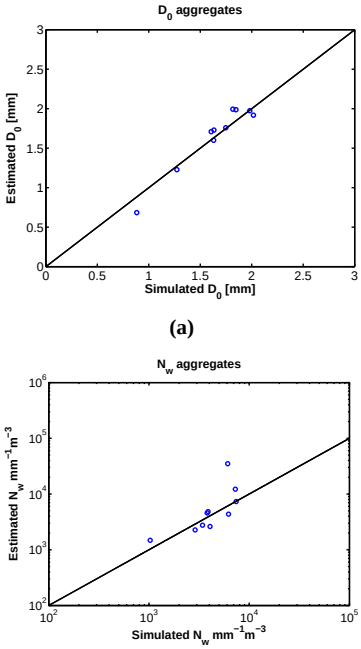

Figure 12: Retrieved values vs input values of DSD parameters of aggregates.

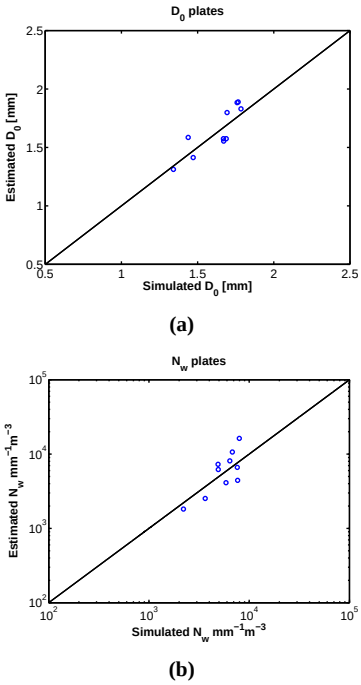

Figure 13: Retrieved values vs input values of DSD parameters of plates

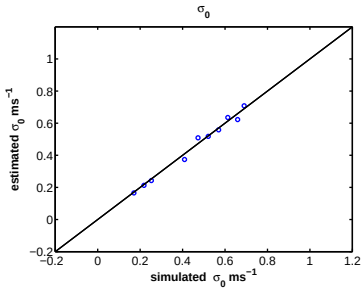

(a)

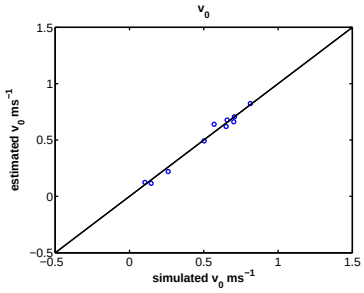

(b)

Figure 14: Retrieved values vs input values of spectral broadening and ambient wind velocity

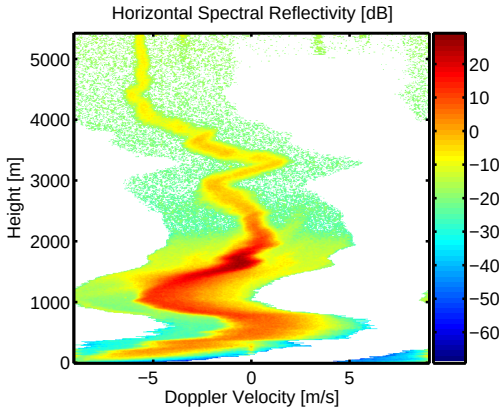

(a)

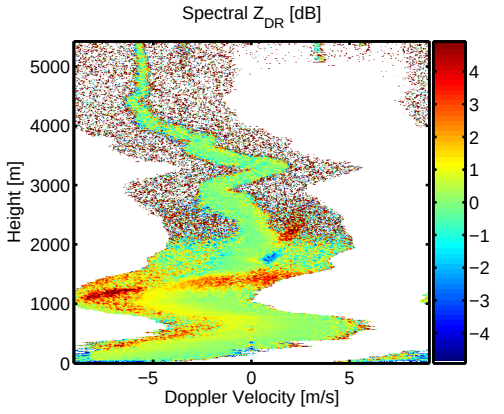

(b)

Figure 15: Spectral radar observables obtained with TARA at September 19^{th}, 2001. a) spectral horizontal reflectivity and b) spectral differential. reflectivity

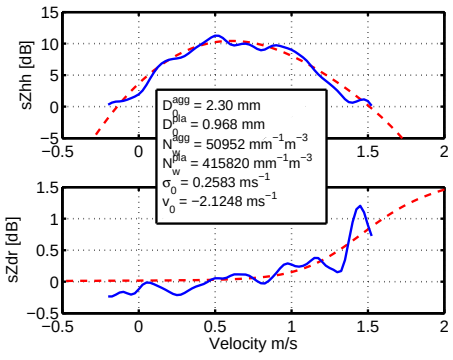

Figure 16: Obtained Doppler spectra at 2036 m with obtained fit. The measurement is given by the solid line and the obtained fit is given with the dashed line.

Netherlands. A moderate rain event is selected with reflectivity values of rain varying from 20 to 35 dBz. The event took place at September 19^{th}, 2001. The elevation angle of the radar was 45 degrees and a range resolution of 15 m was used for the measurement. The measurements are carried out in alternating polarization mode where HH, VV, HV and two offset beams are collected in a block of five sweeps with duration of 1 ms. To calculate 1 Doppler spectrum, 10 spectra are averaged, with each spectrum estimated by applying a 512 sample FFT with a Hamming window. In figure 15 the spectral horizontal reflectivity and spectral differential reflectivity are shown.

The spectra are selected in a range from 150 to 250 m above the top of the melting layer. After clipping the data to remove the noise part of the measurements, the retrieval routine given by (39) is applied on the obtained spectra. In figures 16 - 21 plots are given of the Doppler spectra with the obtained fits.

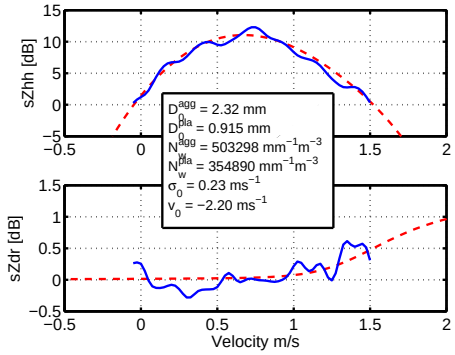

Figure 17: Obtained Doppler spectra at 2057 m with obtained fit. The measurement is given by the solid line and the obtained fit is given with the dashed line.

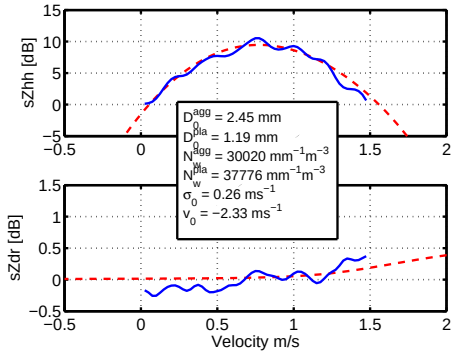

Figure 18: Obtained Doppler spectra at 2078 m with obtained fit. The measurement is given by the solid line and the obtained fit is given with the dashed line.

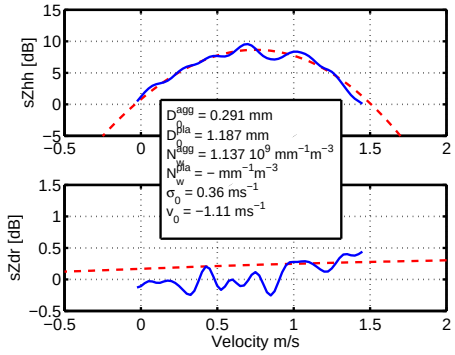

Figure 19: Obtained Doppler spectra at 2100 m with obtained fit. The measurement is given by the solid line and the obtained fit is given with the dashed line.

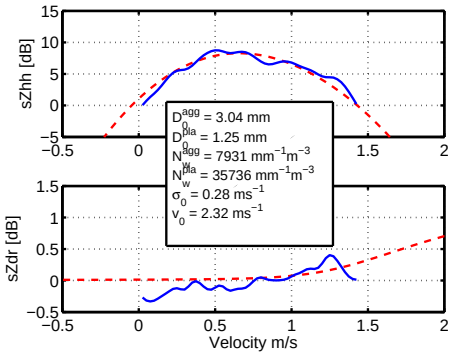

Figure 20: Obtained Doppler spectra at 2121 m with obtained fit. The measurement is given by the solid line and the obtained fit is given with the dashed line.

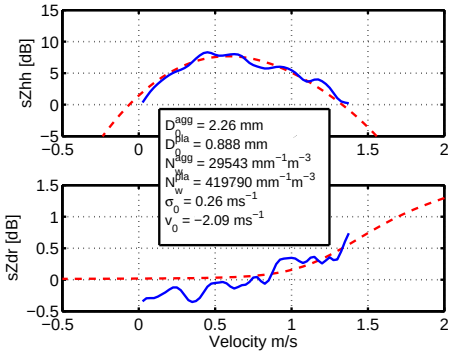

Figure 21: Obtained Doppler spectra at 2142 m with obtained fit. The measurement is given by the solid line and the obtained fit is given with the dashed line.

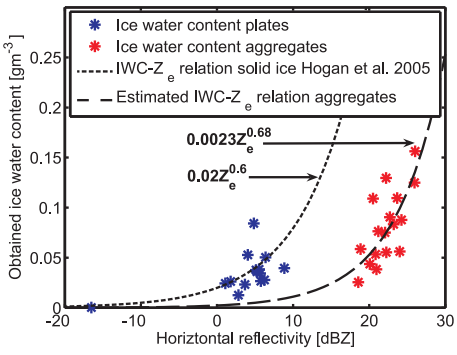

Figure 22: Z-LWC relationships for aggregates and solid ice

4.1 *Discussion*

To be able to draw conclusions on the retrieved values by the retrieval algorithm, it is necessary to calculate an integral parameter, like the Ice Water Content. This is due to the fact that there is little knowledge on microphysical properties of ice crystals above the melting layer in stratiform precipitation. The Ice Water Content is given by (Hogan et al. 2005),

$$\text{IWC} = \int_0^\infty N(D)m(D)dD = \alpha\beta N_w(\frac{D_0}{3.67})^{\beta+1} \tag{40}$$

Table 3: Values of measured reflectivity values and retrieved Ice Water Content for spectra given in figures 16-21

Height [m]	Z_e [dBz]	Z_{DR} [dB]	IWC [gm^{-3}]
2036.5	26.0	0.071	0.6199
2057.7	26.3	0.004	0.6954
2078.9	24.8	0.007	0.4315
2100.1	24.3	0.047	21.436
2121.3	23.8	-0.03	0.2275
2142.5	23.0	-0.02	0.3486

with IWC, the Ice Water Content [kg m^{-3}], N_w in m^{-4} and D_0 in m. α and β are the parameters of the exponential mass-diameter power law given in (11). To obtain the total Ice Water Content a summation has to be done over (40) for plates and aggregates. In table 3 the values for the Ice Water Content obtained with the retrieved DSD values are given.

From the retrieved Ice Water Content values it is noticed, the optimization on the fourth measurement (height 2100.1 m, figure 19) is conspicuous. A reason can be found in the value of sZ_{DR}. Because the retrieval routine is based on this radar parameter it is necessary that the value of sZ_{DR} is significant. In the case of the fourth measurement the sZ_{DR} looks very noisy and will therefore be neglected.
Because the value and shape of sZ_{DR} is important, the focus will be on the first, second and sixth measurement (figures 16, 17 and 21), because the value of sZ_{DR} exceeds 0.5 dB in those cases. Regarding the retrieved values some conclusions can be drawn,

- First of all, the retrieval algorithm is stable. This is seen from the correlation of retrieved values.
- There is a relation between the equivalent reflectivity and the Ice Water Content. If the reflectivity decreases, the Ice Water Content decreases as well. Which is obvious because a smaller reflectivity means less or smaller particles, so less ice will be present in the volume. The reflectivity is mainly dependent on the DSD values for aggregates and it is good to notice the correspondence of this hypothesis with the retrieved values for D_0^{agg} and N_w^{agg}.
- The values for the retrieved N_w are quite high. This has its explanation in the value of sZ_{HH}. If the level of sZ_{HH} of the model is compared to the level of sZ_{HH} in the measurement (figures 8-10 and 16-21) it is noticed there is a significant difference. This difference has its influence on the scaling parameter N_w. Two reasons can explain this difference
  - Some large particles are present in the radar volume. This doesn't effect the mean volume diameter, however they are 'replaced' by a large number of small particles to take into account there large reflectivity
  - The spectra are selected too close to melting layer and melted particles are present in the radar volume as well.

Finally the relationships between the radar reflectivity factor and ice water content are calculated (Figure **??**). Note the good agreement between the Hogan's relationship of solid ice and the retrieved one.

5 CONLUSIONS

The goal of the research is to use dual polarization spectral analysis to retrieve drop size distributions of precipitation above the melting layer. Therefore a literature study is carried out to get insight in the microphysical properties of typical types of snow particles; plates, dendrites, aggregates, graupel and hail. Based on this research, radar cross-sections are calculated and a selection is made on the types of snow particles that dominate the radar retrievals. This assumption is also based on the fall velocity of the different particle types. It is observed that the backscattering of plates and aggregates dominate spectral radar measurements.

A dual polarization spectral analysis is carried out to investigate the dependence of the spectral radar

retrievals sZ_{HH} and sZ_{DR} on the drop size distribution parameters of plates and aggregates. With this knowledge, a retrieval technique is developed which estimates the parameters of the drop size distributions, the spectral broadening factor and the ambient wind velocity. The routine uses a least squares minimization. The developed retrieval technique is illustrated on real measurements as well. It is noticed the measurements must contain significant values for sZ_{DR}, if not the retrieved values will be unreliable.

The work presented in this article shows, that with the addition of spectral analysis it is possible to differentiate between different types of snow particles. It also demonstrates that it is possible to estimate the parameters of their drop size distributions.

Appendix

Table 4: Parameters of the shape-diameter relations for different ice crystals given by (1). Data taken from (Matrosov et al. 1996), (Auer and Veal 1970) and (Bringi and Chandrasekar 2001).

	Size [cm]		Shape	
	from	to	ξ	ζ
Plates	0.0015	0.3	0.0141	0.449
Dendrites	0.03	0.4	0.00902	0.377
Aggregates	0.05	0.8	0.8	1
Hail	0.5	2.5	0.8	1

Table 5: Parameters of the density-diameter relations for different ice crystals given by (3). Data taken from (Pruppacher and Klett 1978), (El-Magd et al. 2000) and (Fabry and Szymer 1999).

	Size [cm]		Density	[gcc^{-1}]
	from	to	k	l
Plates	0.0015	0.3	0.9	0
Dendrites	0.03	0.4	0.2468	-0,377
Aggregates	0.05	0.8	0.015	-1
Graupel	0.2	0.8	0.55	0
Hail	0.5	2.5	0.9	0

Table 6: Parameters of the mass-diameter relations for different ice crystals given by (11). Data taken from (Mitchell 1996) and (Heymsfield and Kajikawa 1987).

	Size [cm]		Mass	[g]
	from	to	α	β
Plates	0.0015	0.3	0.00739	2.45
Dendrites	0.03	0.4	0.003	2.3
Aggregates	0.05	0.8	0.003	2.1
Graupel	0.2	0.8	0.049	3.06
Hail	0.5	2.5	0.466	3

Table 7: Parameters of the area-diameter relations for different ice crystals given by (12). Data taken from (Mitchell 1996) and (Heymsfield and Kajikawa 1987).

	Size [cm]		Area	[cm^2]
	from	to	γ	σ
Plates	0.0015	0.01	0.24	1.85
Plates	0.01	0.3	0.65	2
Dendrites	0.03	0.4	0.21	1.76
Aggregates	0.05	0.8	0.2285	1.88
Graupel	0.2	0.8	0.5	2
Hail	0.5	2.5	0.625	2

References

Auer, A. H. and D. L. Veal, 1970: The dimension of ice particles in natural clouds. *Journal of the atmospheric sciences*, **27**, 919–926.

Bringi, V. N. and V. Chandrasekar, 2001: *Polarimetric Doppler Weather Radar, Principles and applications*. Cambridge University.

Chandrasekar, V., V. N. Bringi, and P. J. Brockwell, 1986: Statistical properties of dual-polarized radar signals. *Preprints 23rd Conf. Radar Met., AMS, Snowmass*, 193–196.

Cotton, W. R., 2004: Personal discussion during internship at Colorado State University, Ft Collins, CO, USA.

Doviak, R. J. and D. S. Zrnic, 1993: *Doppler Radar and Weather Observations*. Academic Press, London.

El-Magd, A., V. Chandrasekar, V. N. Bringi, and W. Strapp, 2000: Multiparameter radar and in situ aircraft observation of graupel and hail. *IEEE Transactions on geosciences and remote sensing*, **38**, 570–578.

Fabry, F. and W. Szymer, 1999: Modeling of the melting layer. part II: Electromagnetic. *Journal of the atmospheric sciences*, **56**, 3593 – 3600.

Gold, L. W. and B. A. Power, 1954: Dependence of the forms of natural ice crystals on meteorological conditions. *Journal of meteorology*, **11**, 35–42.

Heijnen, S. H., L. P. Lighthart, and H. W. J. Russchenberg, 2000: First measurements with TARA; an S-Band Transportable Atmospheric Radar. *Phys. Chem. Earth (B)*, **25**, 995–998.

Heymsfield, A. J. and M. Kajikawa, 1987: An improved approach to calculating terminal velocities of plate-like crystals and graupel. *Journal of the atmospheric sciences*, **44**, 1088–1099.

Hogan, R. J., M. P. Mittermaier, and A. J. Illingworth, 2005: The retrieval of ice water content from radar reflectivity factor and temperature and its use in evaluating a mesoscale model. *Journal of applied meteorology*, **44**, 860–875.

Khvorostyanov, V. I. and J. A. Curry, 2002: Terminal velocities of droplets and crystals: Power laws with continuous parameters over the size spectrum. *Journal of the atmospheric sciences*, **59**, 1872–1844.

Magono, C. and C. W. Lee, 1966: Meteorological classification of natural snow crystals. *Journal of Faculty of Science, Hokkaido University*, **2**, 321–335.

Matrosov, S. Y., R. F. Reinking, R. A. Knopfli, and B. W. Bartram, 1996: Estimation of hydrometeor types and shapes from radar polarization measurements. *Journal of atmospheric and oceanic technology*, **13**, 85 – 96.

Mishchenko, M. I., J. W. Hovenier, and L. D. Travis, 2000: *Light scattering by non spherical particles, theory, measurements and applications*. Academic Press.

Mitchell, D. L., 1996: Use of mass- and area-dimensional power laws for determining precipitation particle terminal velocities. *Journal of the atmospheric sciences*, **53**, 1710 – 1723.

Mitchell, D. L., R. Zhang, and R. L. Pitter, 1990: Mass dimensional relationships for ice particles and the influence of riming on snow flakes. *Journal of applied meteorology*, **29**, 153–163.

Pruppacher, H. R. and J. D. Klett, 1978: *Microphysics of clouds and precipitation*. Reidel Publishing Company, Dordrecht.

Rajopadhyaya, D. K., P. T. May, and R. A. Vincent, 1994: The retrieval of ice particle size information from vhf wind profiler Doppler spectra. *Journal of the atmospheric sciences*, **11**, 1559 – 1568.

Ray, P. S., 1972: Broadband complex refractive indices of ice and water. *Applied Optics*, **11**, 1836 – 1844.

Russchenberg, H. W. J., 1992: *Ground based remote sensing of precipitation using multi-polarized FM-CW Doppler Radar*. Delft University Press.

Skaropoulos, N. C. and H. W. J. Russchenberg, 2003: Simulations of Doppler spectra in the melting layer of precipitation. *Geophysical Research Letters*, **30**, Art. No. 1634.

Szymer, W. and I. Zawadzki, 1999: Modeling of the melting layer. part I: Dynamics and microphysics. *Journal of the atmospheric sciences*, **56**, 3573 – 3592.

Wang, P. K., 1982: Mathematical description of hydrometeors. *Journal of the atmospheric sciences*, **39**, 2615 – 2622.